

Surface and bulk electronic structures of LaOFeAs studied by angle resolved photoemission spectroscopy

L. X. Yang¹, B. P. Xie^{1,*}, Y. Zhang¹, C. He¹, Q. Q. Ge¹, X. F. Wang², X. H. Chen², M. Arita³, J. Jiang³, K. Shimada³, M. Taniguchi³, I. Vobornik⁴, G. Rossi^{4,5}, J. P. Hu⁶, D. H. Lu⁷, Z. X. Shen⁷, Z. Y. Lu⁸, and D. L. Feng^{1†}

¹ State Key Laboratory of Surface Physics, Department of Physics,

and Advanced Materials Laboratory, Fudan University, Shanghai 200433, P. R. China

²Hefei National Laboratory for Physical Sciences at Microscale and Department of Physics,

University of Science and Technology of China, Hefei, Anhui 230026, P. R. China

³Hiroshima Synchrotron Radiation Center and Graduate School of Science, Hiroshima University, Hiroshima 739-8526, Japan

⁴CNR-INFM, TASC Laboratory AREA Science Park – Basovizza, 34012, Trieste, Italy

⁵Dipartimento di Fisica, Universita di Modena e Reggio Emilia, Via Campi 213/A, I-41100 Modena, Italy

⁶Department of physics, Purdue University, West Lafayette, Indiana 47907, USA

⁷Stanford Synchrotron Radiation Lightsource, SLAC National Accelerator Laboratory,

2575 Sand Hill Road, Menlo Park, CA 94025, USA and

⁸Department of Physics, Renmin University of China, Beijing 100872, P. R. China.

(Dated: November 6, 2018)

The electronic structure of LaOFeAs, a parent compound of iron-arsenic superconductors, is studied by angle-resolved photoemission spectroscopy. By examining its dependence on photon energy, polarization, sodium dosing and the counting of Fermi surface volume, both the bulk and the surface contributions are identified. We find that a bulk band moves toward high binding energies below structural transition, and shifts smoothly across the spin density wave transition by about 25 meV. Our data suggest the band reconstruction may play a crucial role in the spin density wave transition, and the structural transition is driven by the short range magnetic order. For the surface states, both the LaO-terminated and FeAs-terminated components are revealed. Certain small band shifts are verified for the FeAs-terminated surface states in the spin density wave state, which is a reflection of the bulk electronic structure reconstruction. Moreover, sharp quasiparticle peaks quickly rise at low temperatures, indicating of drastic reduction of the scattering rate. A kink structure in one of the surface band is shown to be possibly related to the electron-phonon interactions.

I. INTRODUCTION

The discovery of superconductivity in $\text{LaO}_{1-x}\text{F}_x\text{FeAs}$ has declared the advent of iron-based high temperature superconductors (Fe-HTSC's).¹⁻³ Resembling the cuprates, superconductivity emerges from the anti-ferromagnetic (AFM) ordered ground state upon proper doping.²⁻⁵ The intimate relationship between superconductivity and magnetism makes it critical to study the magnetic fluctuations in the parent compounds. On the other hand, the isotope effects,⁶ along with the ubiquitous co-occurrence of the structural and magnetic transitions, allude to the relevance of the lattice degree of freedom for the Fe-HTSC physics. Therefore, it is indispensable to reveal the origin of the structural transition and its effects on the electronic structure as well as the role of phonons for a comprehensive understanding of the Fe-HTSC's. After intensive research, the record superconductivity transition temperature (T_c) of Fe-HTSC's is still held by the $\text{LnO}_{1-x}\text{F}_x\text{FeAs}$ ($\text{Ln}=\text{La}$, Sm , and Ce etc, the so called “1111” series.) systems.^{7,8} Moreover, the divergence of the structural and spin density wave transitions in parent compounds of the “1111” series provides a rare opportunity to unveil these crucial problems.⁹

Angle-resolved photoemission spectroscopy (ARPES) has been employed to study the electronic structure of various Fe-HTSC's, revealing the electronic structure, superconducting gap and the electron-boson coupling.¹⁰⁻¹⁸ However, due to the covalent La-O bonding, LnOFeAs exposes a polar surface with charge redistribution after cleavage.^{10,19,20} Indeed, a recent detailed band calculation of LaOFeAs shows that the

electronic structure of the surface deviates strongly from that of the bulk, and there are two types of surfaces: the LaO-terminated surface and the FeAs-terminated one.²¹ ARPES is essentially a surface probe, therefore, the bulk electronic structure of LnOFeAs is still not definite. This prevents the understanding of this very first and probably the highest- T_c series of iron pnictides, which in turn hampers the construction of a global picture of electronic structure in iron pnictides.

In this Article, we report the ARPES measurements of the electronic structure of LaOFeAs, a parent compound of the “1111” series of iron pnictides. By carefully conducting photon energy dependence and Na-dosing dependence studies on the complicated electronic structure, we could distinguish states from the bulk and the surface. As a result, the nature of the spin density wave (SDW) state is exposed by the bulk bands. Similar to BaFe_2As_2 and other members in the “122” series, no energy gap related to nesting is observed at the Fermi surfaces¹⁴⁻¹⁷. Instead, a band at high binding energies shifts down by about 25 meV, starting from the structural transition temperature. This has been observed recently in NaFeAs by the authors,²² where the fluctuating magnetic order was shown to appear at the structural transition and drive the structural order. Our results on LaOFeAs further suggest that the SDW picture established in the “122” and “111” series applies in the “1111” series as well. The reconstruction (or shift) of the band structure effectively saves the energy, and thus plays a crucial role in driving the SDW transition. Furthermore, we observed drastically rising coherent quasiparticles, which indicates that scattering is strongly suppressed at low temperatures. A kink in dispersion related to possible sur-

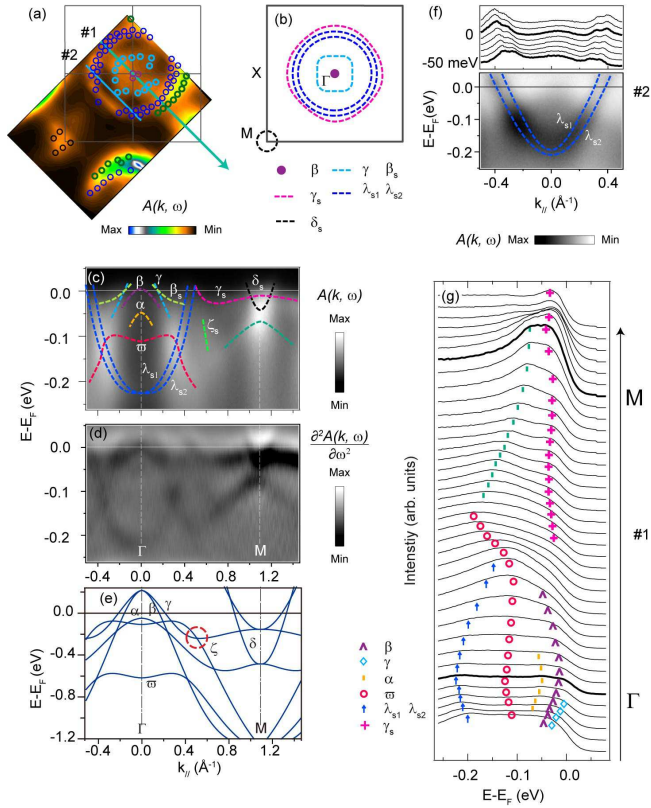


FIG. 1: (color online) Fermi surface mapping and band structure of LaOFeAs along Γ - M in normal state (170 K). (a) ARPES intensity map in the Brillouin zone (BZ) integrated over ± 5 meV around the Fermi energy (E_F), overlaid by the Fermi crossings. (b) The Fermi surfaces are constructed by tracking the Fermi crossings. (c) Photoemission intensity plot along Γ - M (cut 1 in panel (a)). The dashed curves are the guides to eyes obtained by tracking the local minimum locus of second derivative of the raw data with respect to energy as shown in panel (d). (e) The calculated bulk electronic structure of LaOFeAs along Γ - M based on density functional theory. (f) The momentum distribution curves (MDC's) (upper panel) and photoemission intensity plot divided by the resolution convoluted Fermi-Dirac function (lower panel) along cut 2 as marked in panel (a). (g) The corresponding energy distribution curves (EDC's) along Γ - M . Data were taken using 24 eV circularly polarized photons.

face electron-phonon interactions is observed as well.

II. EXPERIMENTAL

High quality LaOFeAs single crystals were synthesized by NaAs-flux method as described elsewhere.²³ Resistivity data confirmed the SDW transition at $T_N=138$ K.⁹ ARPES measurements were conducted at Beamline 9 of Hiroshima synchrotron radiation center (HSRC) with circularly polarized photons and a Scienta R4000 electron analyzer. The Polarization and photon-energy dependence measurements were performed at Beamline 1 of HSRC and the APE Beamline in Elettra synchrotron light source. The energy resolution is 9 meV at Beamline 9, and 20 meV at Beamline 1 and APE,

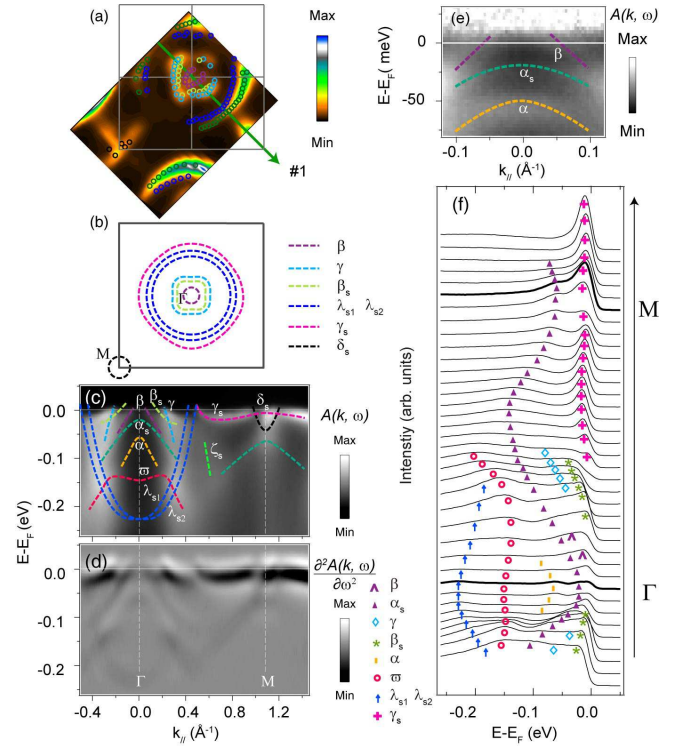


FIG. 2: (color online) Fermi surface mapping and band structure along Γ - M of LaOFeAs in the SDW state (10 K). (a) ARPES intensity map in the BZ integrated over ± 5 meV around E_F , overlaid by the Fermi crossings. (b) The Fermi surfaces are constructed by tracking the Fermi crossings. (c) Photoemission intensity plot along Γ - M (cut 1 in panel (a)). The dashed curves are the guides to eyes obtained by tracking the local minimum locus of second derivative of the raw data with respect to energy as shown in panel (d). (e) The photoemission intensity plot after each MDC is normalized by its integrated weight. (f) The corresponding EDC's along Γ - M . Data were taken using 24 eV circularly polarized photons.

respectively. The overall angular resolution is about 0.3° . All samples were cleaved *in situ* and the ARPES measurements were carried out under ultra-high-vacuum better than 3.0×10^{-11} mbar at Beamline 9 and 5×10^{-11} mbar at Beamline 1 of HSRC. Data were taken within 6 hours after cleavage to minimize the aging effect.

The energy of photons in the experiments ranges from 19 to 64 eV, which gives an electron escape depth of about 5-10 Å according to the universal curve of the electron mean free path in solid. This corresponds to the first two or three layers of LaO or FeAs plane in LaOFeAs. An inner potential of 16 eV is chosen to determine the k_z of the high symmetry points of the Brillouin zone in the photon energy dependence studies.

III. DATA ANALYSIS AND DISCUSSION

A. Normal state electronic structure

The electronic structure in normal state (170 K) are presented in Fig. 1. Photoemission intensities are integrated over a [-5 meV, +5 meV] window at E_F to acquire Fermi surface as shown in Figs. 1(a) and 1(b). The observed Fermi surface consists of three hole pockets, two electron pockets and a tiny patch like feature around the Γ point as well as one electron pocket around M . This is very different from the calculated bulk electronic structure and what is observed in other iron pnictides.^{24,25} The band structure as indicated by the dashed curves in Fig. 1(c) is resolved by tracking the local minimum locus in the second derivative of the ARPES intensity plot with respect to energy (Fig. 1(d)) and confirmed by the peaks in the corresponding energy distribution curves (EDC's) as shown in Fig. 1(g). The top of the β band touches the E_F and forms a Fermi patch near Γ . The Fermi crossings of γ and β_s nearly coincide, forming two hole pockets of the Fermi surface. Two parabolic electron bands λ_{s1} and λ_{s2} contribute two electron Fermi pockets around Γ . A weak but resolvable feature α shows up with its top at about 50 meV below E_F . The flat γ_s band contributes one large hole pocket around Γ which is much larger than the corresponding bulk Fermi surface in the calculation. Around the M point, only one electron band could be clearly resolved. Note that the petal like feature around M in Fig. 1(a) stems from the remnant spectral weight of the flat γ_s band, instead of Fermi crossings.

The overall measured electronic structure of LaOFeAs deviates strongly from that of other pnictides and the calculations as shown in Fig. 1(e).^{14,24-26} In total, we observed 9 bands and 5 Fermi surface sheets around Γ (actually, another hole like band α_s could be resolved around Γ at low temperature as shown below.) instead of 6 bands and 2 Fermi surface sheets in the bulk band calculations. This complication can be qualitatively explained by the recent calculations of the surface and bulk band structures of LaOFeAs.²¹ Because of the strong La-O or Fe-As covalent bonding, the surface is either an FeAs or a LaO plane. The polarity of the surface causes significant lattice relaxation and charge redistribution to minimize its static electric energy and thus changes the electronic structure dramatically.^{10,11} As a result, the FeAs-terminated surface is electron-deficient, while the LaO-terminated surface is electron-excess. As ARPES probes only 5~10 Å with the photon energies exploited here, the measured electronic structure are contributed from the first 2 or 3 LaO or FeAs planes. Because the two types of surfaces could coexist on a single cleaved sample, and the FeAs plane underneath the LaO surface is different from the FeAs surface plane, they conspire to construct the complicated band structure in the experimental data.

The surface band calculations (Ref.21) clearly predicted that the excess electrons in the surface LaO plane reside in the La $5d + 6s$ states, and give a large electron pocket around Γ . However, instead of one pocket, we have observed two large electron pockets (λ_{s1} and λ_{s2}), which could be resolved more clearly in Fig. 1(f). Since the observed two bands

mimic the spin-orbital splitting of the Au(111) surface states, the difference between our data and the predicted ones could be caused by the fact that spin-orbital coupling was not included in the calculation, while the spin-orbital coupling of $5d$ electrons is not negligible.²⁷ For comparison, the momentum splitting of λ_{s1} and λ_{s2} is about 0.03\AA^{-1} and the Rashba energy is merely ~ 1 meV. Correspondingly, the Rashba parameter α_R , *i.e.*, the ratio of the Rashba energy to the momentum splitting, is about $0.023\text{ eV}\text{\AA}^{-1}$. This value is much smaller than that of Au: $\alpha_R=0.33\text{ eV}\text{\AA}^{-1}$,²⁸ but comparable with that of the two dimensional electronic system in the InGaAs/InAlAs heterostructure.²⁹ Furthermore, we note that the occupied bandwidth of λ_{s1} and λ_{s2} is about 0.22 eV, which is similar to the calculation (0.2 eV), indicating weak correlations in the LaO layer, in contrast to the FeAs bands.³⁰

B. SDW state electronic structure

Figure 2 displays the corresponding electronic structure in the SDW state. For the Fermi surface as shown in Figs. 2(a) and 2(b), the tiny patch like feature at Γ evolves into a small hole pocket. The Fermi crossings of the γ and β_s bands does not coincide any more, forming two hole pockets around the Γ point. The size of γ pocket expands about 70% at low temperature. There is little change of the other Fermi surface sheets. The band structure along Γ - M is shown in the ARPES intensity plot (dashed curves in Fig. 2(c)) and its second derivative with respect to energy (Fig. 2(d)). An additional hole like band (α_s) with its band top at about -20 meV could be resolved in the Fig. 2(e). The reason that α_s was not resolved at high temperatures might be due to thermal broadening. The splitting of the λ_{s1} and λ_{s2} bands is independent of temperature, which is expected for spin orbital splitting. The α and ϖ bands move about 5 meV and 30 meV downward respectively, saving the total energy of the system. The γ_s band moves about ~ 5 meV towards E_F , sharpening the petal like feature around the M point without additional Fermi crossing of the γ_s band. No clear variation of the electron band around M is found. Moreover, no energy gap related to Fermi surface nesting was observed, similar to the case of the "122", "111" and "11" series.^{14-17,22,30}

C. Polarization dependence

The multiband nature of the iron pnictides leads to complex band structure, and the additional surface states make it even more complicated in LaOFeAs. Since the band structure shows strong polarization dependence, we conducted polarization dependent ARPES measurements to further resolve the band structure. Fig. 3(a) displays the definition of two different experimental geometries according to the linear polarization of the incoming photons. The incident beam and the sample surface normal define a mirror plane. For the σ (or π) experimental geometry, the electric field of the incident photons is out of (or in) the mirror plane. The matrix element for the photoemission process could be described as

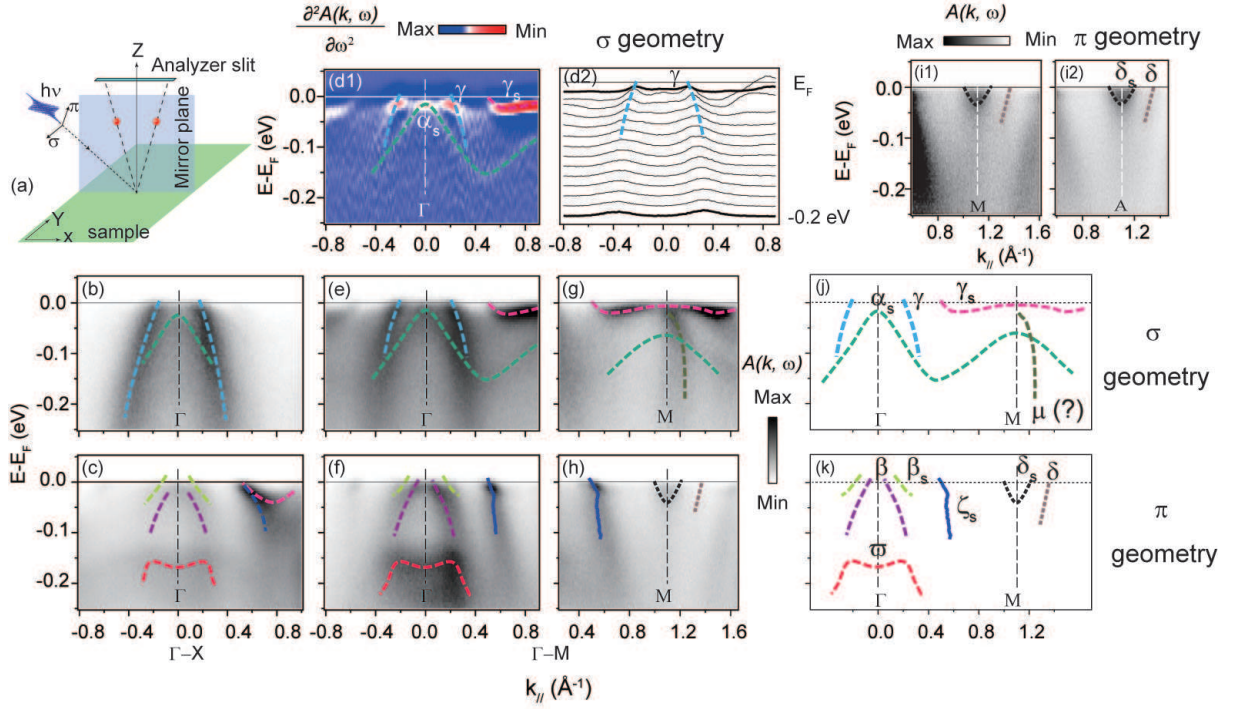


FIG. 3: (color online) Polarization dependent measurements along high symmetry directions. (a) Schematic diagram of two types of experimental setups. (b)-(c) ARPES intensity plot along Γ -X (d1) The second derivative of ARPES intensity plot with respect to energy and (d2) the corresponding MDC's along Γ -M. (e)-(h) ARPES intensity plot along Γ -M. (i1)-(i2) ARPES intensity plot around the M and A points. The contrast of the images is adjusted to show the δ band more clearly. (j) and (k) summarize the band structure extracted for the corresponding polarizations. The dashed curves in the photoemission intensity plots are the guides to eyes. The geometry of experimental setups are marked on the top or right of the panels. The corresponding photon energies for the Γ , M and A points are 59 eV, 43 eV and 33 eV respectively to reach the right k_z . Data were taken at 10 K.

$$M_{f,i}^k \propto |\langle \Psi_f^k | \hat{\epsilon} \cdot \mathbf{r} | \Psi_i^k \rangle|^2$$

Since the final state Ψ_f of photoelectrons could be approximated by a plane wave with its wave vector in the mirror plane, Ψ_f is always even in our experimental geometry. In the σ (or π) geometry, $\hat{\epsilon} \cdot \mathbf{r}$ is odd (or even) with respect to the mirror plane. Thus, only the odd (or even) component of the initial state Ψ_i could show up in the photoemission data.³⁰

The photoemission intensity plot along high symmetry directions are shown in Figs. 3(b)-(c) and (e)-(h). The dashed lines are the guides to eyes while the solid curves are the fitting of MDC's peaks. Around the Γ point, the β and β_s (α_s and γ) bands only shows up in π (σ) geometry of experimental setup, exhibiting their even (odd) nature with respect to the mirror plane. The flat γ_s band is absent in σ (π) geometry along Γ -X (Γ -M). It exhibits different parity in two high symmetry directions. The ϖ band could be observed only in π geometry along both directions. Its parity is analogous to that of the d_{z^2} band as predicted in density functional theory.³⁰ Fig. 3(d1) shows that the α_s band disperses from Γ to M and connects smoothly with the hole like band there. Around M point, the δ and δ_s bands only shows up in the π experimental geometry, indicating their even parities. The contrast of the ARPES intensity plots around M and A are adjusted to

show the δ band more clearly in Figs. 3(i1) and (i2). Note that we observed a fast dispersed hole like band μ around the M point, whose origin is still not clear yet (Fig. 3(g)). We have reproduced the obtained band structure under different experimental geometries in Figs. 3(j) and (k) to summarize the band structure along Γ -M.

An interesting result in Figs. 3(f) and 3(h) is the kink like dispersion of the ζ_s band, which has been reported earlier in CeOFeAs as well.²⁰ The dispersion of the ζ_s band is tracked by fitting its MDC's (the blue solid curve). A kink does appear at about -30 meV, which might indicate strong electron-phonon interactions for this particular band. However, band crossings could cause similar structure. A kink could be possibly introduced by the hybridization of the γ_s and ζ_s bands as highlighted by the red dashed circle in Fig. 1(e), there might be a band crossing in this momentum region. Correspondingly, the γ_s band should connect either to the γ or the β_s band to hybridize with the ζ_s band. However, the γ band could be clearly resolved to disperse quickly downward from the MDC's in Fig. 3(d2), it could not connected to the γ_s band. On the other hand, β_s and γ_s have the opposite parities as shown in Figs. 3(j) and (k). Based on LDA calculations and our previous studies of the orbital nature of bands in $\text{BaFe}_{2-x}\text{Co}_x\text{As}_2$,³¹ a band should not change its parity in such a small momentum range. Therefore, β_s and γ_s bands could not be from the same

band. In conclusion, the polarization data further confirms that the kink is not caused by a band crossing, but most likely intrinsic electron-phonon interactions.

D. Identification of surface and bulk electronic structure: k_z dependence and Na dosing effects

It is crucial to identify the bulk and surface bands to reveal the intrinsic response of the electronic structure to the phase transitions. Photon-energy dependence measurements were carried out for this purpose, because different photon energies correspond to different k_z , and only bulk bands could exhibit k_z -dispersion. Under the π geometry of experimental setup, as shown in Figs. 4(a) and 4(b), only the ϖ band has noticeable k_z dependence as its energy position at $k_{\parallel} = 0$ changes with the variation of photon energy. Thus, it should be one of the bulk bands. No clear k_z dependence is observed for the bands crossing E_F according to the photon energy dependence of the MDC's at E_F as shown in Fig. 4(b). For the bands observed under σ experimental geometry, only weak k_z dependence could be verified for the γ band from the MDC's at E_F as shown in the Fig. 4(f). No other bands show noticeable k_z dependence as shown by the EDC's at $k_{\parallel} = 0$, $k_{\parallel} = 1.1\text{\AA}$ and $k_{\parallel} = 0.2\text{\AA}$ (Figs. 4(c)-4(e)). Considering the short electron escape depth, the bulk bands observed here are most likely originated from the FeAs plane below the LaO plane, for which the calculation indicates its carrier concentration is close to that of the bulk.²¹ The k_z dispersion suggests that the band structure quickly becomes bulk-like in the layer just underneath the surface.

For the bands that do not show much k_z dispersion, they could either surface or bulk ones in such a quasi-two-dimensional system. We further explore their reactions to the surface disorder effects through sodium dosing, as the bulk bands are expected to be more robust than the surface ones. The sample was exposed to a Na evaporator at 150 °C for 10 seconds, which would put about 1 monolayer of Na atoms on the surface. Our data indicate that the chemical potential of the system is not changed too much after Na dosing. Thus, we would expect that additional scattering channels are introduced on the surface by the Na dosing, which would dramatically change the surface bands. The data taken at π -geometry before and after the dosing were shown in Fig. 5. Indeed, the bulk ϖ band is barely changed by Na dosing. Consistently, the surface LaO band (λ_{s1} or λ_{s2}) disappeared after Na dosing (Fig. 5(a) and (c)). The β_s and ζ_s bands disappear as well, while the β band survives the dosing. Since the β band reacts to the Na-dosing so differently from the surface bands, we attribute the β band to the bulk, while the β_s and ζ_s bands to the surface FeAs plane. For the A point, only the δ band survives the dosing, indicating its bulk character as shown in Figs. 5(c) and (f).

Due to the surface charge redistribution, calculation shows that the doping concentrations and band structures of the several layers close to surface are different from each other and that in bulk. The surface carrier concentration could be estimated by the Luttinger volume of the relevant Fermi surfaces.

We identify three surface bands crossing Fermi level around Γ , which is consistent with the surface band calculation.²¹ The carrier occupation of the surface β_s , γ_s , ζ_s and δ_s bands is about $4.39 e^-$ per $[\text{Fe}_2\text{As}_2]$ formula unit, smaller than the calculated $4.89 e^-$ (based on the calculated Fermi surface in Ref.21) and expected $6 e^-$ for the bulk bands.¹¹ On the other hand, the counting for the states of LaO layer gives rise to 0.53 excess electrons per $[\text{La}_2\text{O}_2]$ formula unit, larger than the calculated number of $0.25 e^-$ (based on the calculated Fermi surface in Ref.21). The certain difference may be related to the fact that some bands (thus some Fermi pockets) could be missing in the experiments.

E. Shifts in bulk band structure correlated with the SDW transition

The identified bulk bands allow us to investigate the intrinsic bulk response of the electronic structure to the phase transitions. The band structure in the normal state and SDW state are reproduced and overlaid in Fig. 6(a). The ϖ band clearly shifts about 30 meV to high energies, which reduces the total energy of the system effectively and energetically favors the SDW transition. The temperature dependence of EDC's at $k_{\parallel}=0.43 \text{\AA}^{-1}$ are tracked to examine the evolution of the ϖ band. As shown in Fig. 6(b), both the peak position and the leading edge shift about 30 meV towards the high energy from 180 K to 15 K. The shift happens around structural transition and goes through SDW transition smoothly (the inset of Fig. 6(b) and the green triangles in Fig. 6(d)). Since the dispersion of ϖ is concealed by other bands here, data taken with 19 eV photons are presented in Fig. 6(c), where the ϖ band is more enhanced due to certain matrix element effects. The band shift as much as 25 ± 4 meV is quantified by both the peak positions (red circles) and leading edge locations (blue squares) as shown in Fig. 6(e). Data obtained in different ways all show that the band shift indeed starts from the structural transition, and proceeds smoothly across the SDW transition to high energies.

This fact suggests that such band shift is related to the structural transition. However, the 0.52% distortion of the lattice could only account for about 4 meV band shift, which is far too less than the observation. On the other hand, the band shift could be related to the magnetic ordering considering its same energy scale as the magnetic exchange interactions.^{14,15,17,22} Therefore, the smoothly evolution of the band shift across the SDW transition could be interpreted that there is already SDW fluctuation or short range magnetic order at the structural transition. Particularly, such a shift of band at the structural transition temperatures has been observed in NaFeAs before.²² Furthermore, it has been proved that a short range magnetic order emerges around the structural transition temperature, since the band folding due to such an order is observed starting from the structural transition temperature.²² Therefore, the band shift in NaFeAs and LaOFeAs can be directly associated with the SDW fluctuations. Coincidentally, it has been proposed that the magnetic fluctuations could drive the structural transition.³² Our result provides direct support for such a sce-

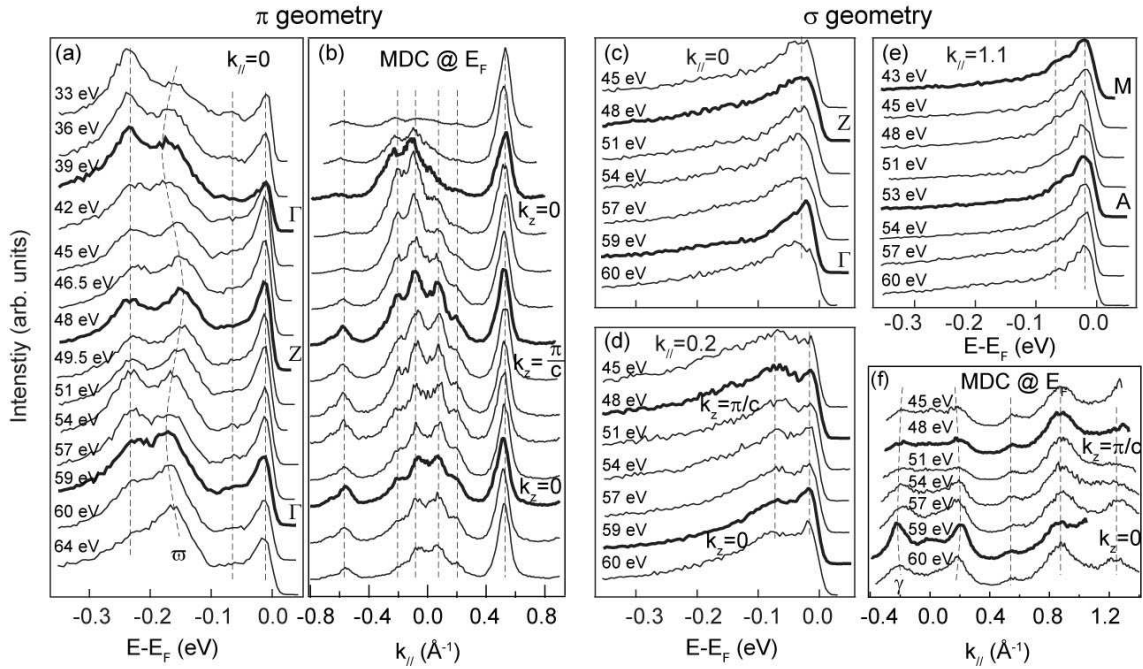


FIG. 4: (color online) Photon energy dependence of (a) the EDC's at in-plane momentum $k_{\parallel} = 0$, and (b) the MDC's at E_F . The EDC's at in-plane momentum (c) $k_{\parallel} = 0$, (d) $k_{\parallel} = 0.2 \text{ \AA}^{-1}$ and (e) $k_{\parallel} = 1.1 \text{ \AA}^{-1}$. (f) the MDC's at E_F . Data in panel (a) and (b) were taken under π geometry, while data in panel (c)-(e) were taken under σ geometry of experimental setup. The in-plane projection are along the Γ - M direction. Data were taken at 10K.

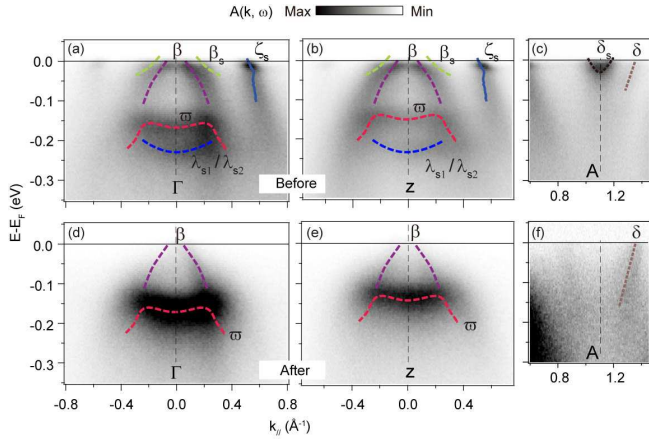


FIG. 5: (color online) Photoemission intensity plots along (a) the Γ - M direction, (b) the Z - A direction and (c) the Z - A direction under π geometry of experimental setup as in Fig. 3(a). (d)-(f) After the sample was exposed to Na dosing, data were taken at the same condition as panels a and b respectively. The dashed curves are the guides to eyes. Data were taken at 10 K under π experimental geometry. The corresponding photon energies for the Γ , Z and A points are 59 eV, 48 eV, and 33 eV, respectively.

nario in the “1111” series of iron pnictides. Moreover, the observed shift of bands at high binding energies is consistent with the reconstruction of the electronic structure in the parent compounds of “122” series evolving to the SDW state.¹⁴⁻¹⁷ Therefore, our observation of the band shift in LaOFeAs sup-

ports the electronic structure reconstruction as the mechanism for SDW. It might allude to the existence of an electronic nematic phase in the “1111” series between structural and SDW transition as proposed in Ref.32.

F. Drastic temperature dependence of quasiparticles

To further investigate the influence of the structural and SDW transitions on electronic structure, the sharp quasiparticle peaks at low temperatures as shown in Fig 2(f) are examined as a function of temperature in Fig. 7. At the Γ point (Fig. 7(a)), a prominent coherent quasiparticle peak emerges as temperature decreases, suggesting a rapid decrease of scattering rate. The same behavior could be found at a large portion of Brillouin zone, such as the M point and the location of $k_{\parallel} = 0.75 \text{ \AA}^{-1}$ (Figs. 7(b) and 7(c)). The drastic rising of the quasiparticle peaks is well beyond the thermal sharpening effect at low temperatures. In order to reveal the relation between this anomalous evolution of the quasiparticle peaks and the phase transition, we divide the Fermi-Dirac functions of the temperature dependent EDC's in Fig. 7(c) and fit the quasiparticle peak with a Lorentz function and a linear background as shown in the inset of Fig. 7(c). The quasiparticle peak width which reflects the scattering rate decreases drastically at low temperatures as indicated by the red circles in Fig. 7(d). Such decrease of scattering rate is compatible with that in CeOFeAs,²⁰ except that surface and bulk bands were not distinguished there.

The scattering from spin fluctuations could be dramati-

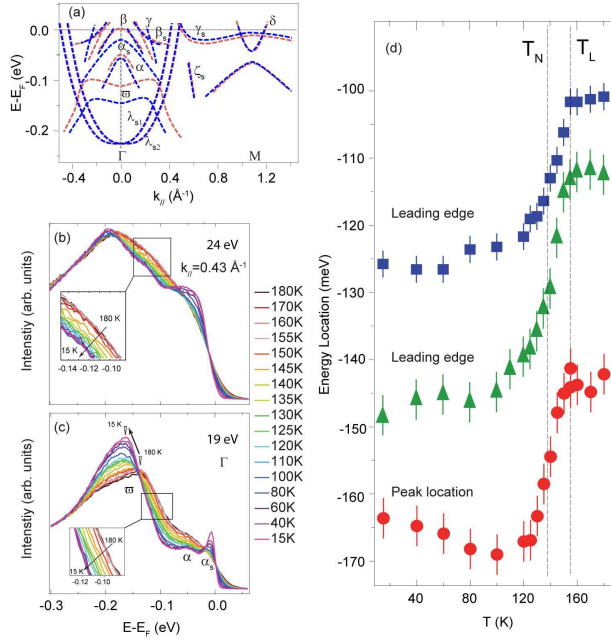


FIG. 6: (color online) The band shift in LaOFeAs. (a) The comparison of the band structure at 170 K (red dashed curves) and 10 K (blue dashed curves) reproduced from Fig 1 and Fig 2. (b)-(c) The temperature dependence of EDC's at (b) $k_{\parallel}=0.43 \text{ \AA}^{-1}$ obtained using 24 eV photons and (c) the Γ point obtained using 19 eV photons. The insets of panel (b) and (c) zooms in the rectangle region to show the leading edge shift more clearly. (d) The green triangles are the leading edge locations of the EDC's corresponding to the ϖ band in panel (b). The blue squares and the red circles are the leading edge and peak locations of the EDC's corresponding to the ϖ band in panel (c).

cally suppressed by the formation of a spin gap below SDW transition.^{33,34} Consistently, the quasi-particle weight near E_F increases at low temperature as shown in Fig. 7(d) (blue squares). Furthermore, the surface is still a quasi two dimensional system, it could be coupled to the bulk, for example, through certain scattering processes. Therefore, the drastic temperature dependence of the surface bands might be related to the SDW transition in the bulk. However, no noticeable anomaly for the evolution of the peak width at SDW transitions is observed. One of the possible relevance is that the magnetic fluctuations happen even above the structural transition. The relationship of this peculiar behavior and the phase transitions needs further studies. Indeed, NMR measurements have verified the change of the fluctuation around structural transition and its suppression at low temperatures although there is a drastic enhancement of the fluctuations around SDW transition.^{35,36}

IV. SUMMARY

To summarize, we have obtained a comprehensive picture of the electronic structure in LaOFeAs by distinguishing bulk (fig.8 (a) curves) and surface bands (fig.8 (b)). The origin of

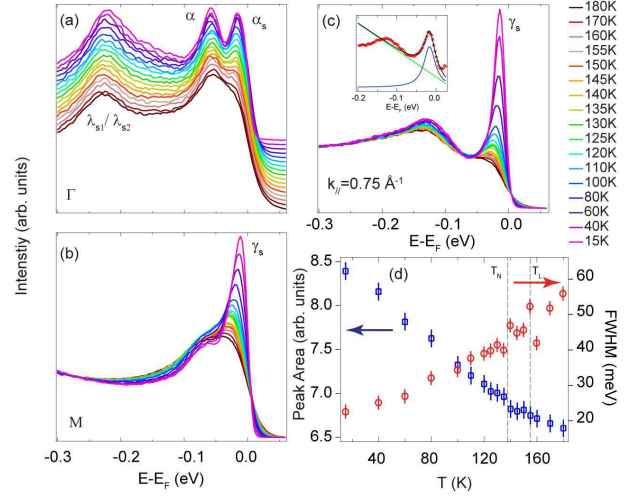


FIG. 7: (color online) The evolution of the electronic structure in LaOFeAs. (a)-(c) Temperature dependence of EDC's with momentum locations at (a) Γ , (b) M and (c) $k_{\parallel}=0.75 \text{ \AA}^{-1}$. The inset of panel (c) shows the fitting of the de-convoluted EDC at 100K. (d) The evolution of the peak area and full width at half maximum (FWHM) of the EDC's in the panel (c). The peak area is obtained by integrating the spectral weight of the EDCs over a window of $[-0.065, 0.05] \text{ eV}$.

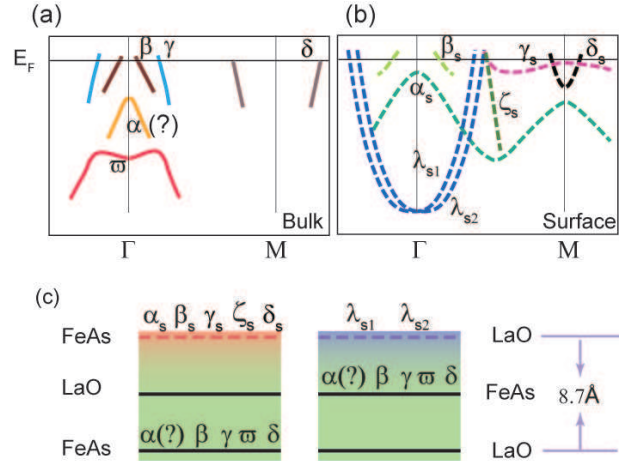


FIG. 8: (color online) The summary of (a) the surface and (b) bulk band structures that can be measured. (c) The diagram for the origin of the measured bands.

the bands is summarized in Fig.8 (c) as well. We note that some certain bands may be missing in the measurements because of the matrix element effects. Due to the charge redistribution effect in the “1111” series, the measured electronic structure of LaOFeAs is heavily contaminated by the surface states. Therefore, great caution has to be taken on ARPES data obtained on this “1111” series of iron pnictides. For example, the measured superconducting gap on a surface band might be caused by the proximity effects, and the strong kink is actually on a surface band, it does not necessarily suggest strong electron-phonon interactions in the bulk bands.

Our data show that the large downward shift of the bulk band saves the total energy of the system and drives the phase

transitions. The onset of this shift at the structural transition temperature further evidence the existence of a fluctuating magnetic ordering phase that drives the structural transition. The results in the “1111” series are consistent with the observations in the “122” and “111” series of iron pnictides, suggesting the universality of the electronic response to the structural and magnetic phase transitions. Our results would

help to construct a global picture of the Fe-HTSC physics.

Acknowledgement: Some preliminary data were taken at beam line 5-4 of Stanford Synchrotron Radiation Laboratory. This work was supported by the NSFC, MOST (National Basic Research Program No.2006CB921300 and 2006CB601002), MOE, and STCSM of China.

- * bpxie@fudan.edu.cn
 † dlffeng@fudan.edu.cn
- ¹ Y. Kamihara, T. Watanabe, M. Hirano and H. Hosono, *J. Am. Chem. Soc.* **130**, 3296 (2008).
 - ² X. H. Chen, T. Wu, G. Wu, R. H. Liu, H. Chen and D. F. Fang, *Nature (London)* **453**, 761 (2008).
 - ³ G. F. Chen, Z. Li, D. Wu, G. Li, W. Z. Hu, J. Dong, P. Zheng, J. L. Luo and N. L. Wang, *Phys. Rev. Lett.* **100**, 247002 (2009).
 - ⁴ Hiroki Takahashi, Kazumi Igawa, Kazunobu Arii, Yoichi Kamihara, Masahiro Hirano, Hideo Hosono, *Nature (London)* **453**, 376 (2008).
 - ⁵ Min Xu, Fei Chen, Cheng He, Hong-Wei Ou, Jia-Feng Zhao and Dong-Lai Feng, *Chem. Mater.* **20**, 7201 (2008).
 - ⁶ R. H. Liu, T. Wu, G. Wu, H. Chen, X. F. Wang, Y. L. Xie, J. J. Ying, Y. J. Yan, Q. J. Li, B. C. Shi, W. S. Chu, Z. Y. Wu and X. H. Chen, *Nature (London)*, **459**, 64 (2008).
 - ⁷ Z. A. Ren, W. Lu, J. Yang, W. Yi, X.-L. Shen, Z. Cai, G.-C. Che, X.-L. Dong, L.-L. Sun, F. Zhou and Z.-X. Zhao, *Chin. Phys. Lett.* **25**, 2215 (2008).
 - ⁸ C. Wang, L.-J. Li, S. Chi, Z.-W. Zhu, Z. Ren, Y.-K. Li, Y.-T. Wang, X. Lin, Y.-K. Luo, S. Jiang, X.-F. Xu, G.-H. Cao and Z. A. Xu, *EPL* **83**, 67006 (2008).
 - ⁹ Clarina de la Cruz, Q. Huang, J. W. Lynn, Jiying Li, W. Ratcliff II, J. L. Zarestky, H. A. Mook, G. F. Chen, J. L. Luo, N. L. Wang and Pengcheng Dai, *Nature*, **453**, 899 (2008).
 - ¹⁰ D. H. Lu, M. Yi, S.-K. Mo, A. S. Erickson, J. Analytis, J.-H. Chu, D. J. Singh, Z. Hussain, T. H. Geballe, R. R. Fisher and Z.-X. Shen, *Nature*, 455, 81 (2009).
 - ¹¹ D.H. Lu, M. Yi, S.-K. Mo, J.G. Analytis, J.-H. Chu, A.S. Erickson, D.J. Singh, Z. Hussain, T.H. Geballe, I.R. Fisher and Z.-X. Shen, *physica C*, **469**, 452 (2009).
 - ¹² H. Ding, P. Richard, K. Nakayama, K. Sugawara, T. Arakane, Y. Sekiba, A. Takayama, S. Souma, T. Sato, T. Takahashi, Z. Wang, X. Dai, Z. Fang, G. F. Chen, J. L. Luo and N. L. Wang, *Euro. Phys. Lett.* **83**, 47001 (2009).
 - ¹³ P. Richard, T. Sato, K. Nakayama, S. Souma, T. Takahashi, Y.-M. Xu, G. F. Chen, J. L. Luo, N. L. Wang and H. Ding, *phys. Rev. Lett.* **102**, 047003 (2009).
 - ¹⁴ L. X. Yang, Y. Zhang, H. W. Ou, J. F. Zhao, D. W. Shen, B. Zhou, J. Wei, F. Chen, M. Xu, C. He, Y. Chen, Z. D. Wang, X. F. Wang, T. Wu, G. Wu, X. H. Chen, M. Arita, K. Shimada, M. Taniguchi, Z. Y. Lu, T. Xiang and D. L. Feng, *Phys. Rev. Lett.* **102**, 107002 (2009).
 - ¹⁵ Y. Zhang, J. Wei, H. W. Ou, J. F. Zhao, B. Zhou, F. Chen, M. Xu, C. He, G. Wu, H. Chen, M. Arita, K. Shimada, H. Namatame, M. Taniguchi, X. H. Chen, D. L. Feng, *Phys. Rev. Lett.* **102**, 127003 (2009).
 - ¹⁶ M. Yi, D. H. Lu, J. G. Analytis, J.-H. Chu, S.-K. Mo, R.-H. He, M. Hashimoto, R. G. Moore, I. I. Mazin, D. J. Singh, Z. Hussain, I. R. Fisher and Z.-X. Shen, *Phys. Rev. B* **80**, 174510 (2009).
 - ¹⁷ Bo Zhou, Yan Zhang, Le-Xian Yang, Min Xu, Cheng He, Fei Chen, Jia-Feng Zhao, Hong-Wei Ou, Jia Wei, Bin-Ping Xie, Tao Wu, Gang Wu, Masashi Arita, Kenya Shimada, Hirofumi Namatame, Masaki Taniguchi, X. H. Chen, and D. L. Feng, *Phys. Rev. B* **81**, 155124 (2010).
 - ¹⁸ M. Yi, D. H. Lu, J. G. Analytis, J.-H. Chu, S.-K. Mo, R.-H. He, R. G. Moore, X. J. Zhou, G. F. Chen, J. L. Luo, N. L. Wang, Z. Hussain, D. J. Singh, I. R. Fisher and Z.-X. Shen, *Phys. Rev. B* **80**, 024515 (2009).
 - ¹⁹ Takeshi Kondo, A. F. Santander-Syro, O. Copie, Chang Liu, M. E. Tillman, E. D. Mun, J. Schmalian, S. L. Budko, M. A. Tanatar, P. C. Canfield and A. Kaminski, *Phys. Rev. Lett.* **101**, 147003 (2008).
 - ²⁰ Haiyun Liu, G. F. Chen, Wentao Zhang, Lin Zhao, Guodong Liu, T.-L. Xia, Xiaowen Jia, Daixiang Mu, Shanyu Liu, Shaolong He, Yingying Peng, Junfeng He, Zhaoyu Chen, Xiaoli Dong, Jun Zhang, Guiling Wang, Yong Zhu, Zuyan Xu, Chuangtian Chen and X. J. Zhou, arXiv:0912.2838 (unpublished).
 - ²¹ H. Eschrig, A. Lankau and K. Koepfner, arXiv:1001.1127 (unpublished).
 - ²² C. He, Y. Zhang, B. P. Xie, X. F. Wang, L. X. Yang, B. Zhou, F. Chen, M. Arita, K. Shimada, H. Namatame, M. Taniguchi, X. H. Chen, J. P. Hu, D. L. Feng, arXiv:1001.2981 (unpublished).
 - ²³ J.-Q. Yan, S. Nandi, J. L. Zarestky, W. Tian, A. Kreyssig, B. Jensen, A. Kracher, K. W. Dennis, R. J. McQueeney, A. I. Goldman, R. W. McCallum, T. A. Lograsso, *Appl. Phys. Lett.* **95**, 222504 (2009).
 - ²⁴ I. I. Mazin, M. D. Johannes, L. Boeri, K. Koepfner and D. J. Singh, *Phys. Rev. B* **78**, 085104 (2008).
 - ²⁵ F. J. Ma and Z.-Y. Lu, *Phys. Rev. B* **78**, 033111 (2008).
 - ²⁶ D. J. Singh, *Phys. Rev. B* **78**, 094511 (2008).
 - ²⁷ B. J. Kim, Hosub Jin, S. J. Moon, J.-Y. Kim, B.-G. Park, C. S. Leem, Jaeyun Yu, T. W. Noh, C. Kim, S.-J. Oh, J.-H. Park, V. Durairaj, G. Cao, and E. Rotenberg, *Phys. Rev. Lett.* **101**, 076402 (2008).
 - ²⁸ H. Cercellier, Y. Fagot-Revurat, B. Kierren, F. Reinert, D. Popović and D. Malterre, *Phys. Rev. B* **70**, 193412 (2004).
 - ²⁹ C. L. Yang, H. T. He, Lu Ding, L. J. Cui, Y. P. Zeng, J. N. Wang and W. K. Ge, *Phys. Rev. Lett.* **96**, 186605 (2006).
 - ³⁰ Fei Chen, Bo Zhou, Yan Zhang, Jia Wei, Hong-Wei Ou, Jia-Feng Zhao, Cheng He, Qing-Qin Ge, Masashi Arita, Kenya Shimada, Hirofumi Namatame, Masaki Taniguchi, Zhong-Yi Lu, Jiangping Hu, Xiao-Yu Cui and D. L. Feng, *Phys. Rev. B* **81**, 014526 (2010).
 - ³¹ Y. Zhang, B. Zhou, F. Chen, J. Wei, M. Xu, L. X. Yang, C. Fang, W. F. Tsai, G. H. Cao, Z. A. Xu, M. Arita, H. Hayashi, J. Jiang, H. Iwasawa, C.H. Hong, K. Shimada, H. Namatame, M. Taniguchi, J. P. Hu, D. L. Feng, arXiv:0904.4022 (unpublished).
 - ³² Chen Fang, Hong Yao, Wei-Feng Tsai, Jiangping Hu and Steven A. Kivelson, *Phys. Rev. B* **77**, 224509 (2008).
 - ³³ Jun Zhao, Dao-Xin Yao, Shiliang Li, Tao Hong, Y. Chen, S. Chang, W. Ratcliff II, J.W. Lynn, H. A. Mook, G. F. Chen, J. L. Luo, N. L. Wang, E.W. Carlson, Jiangping Hu and Pengcheng Dai, *Phys. Rev. Lett.* **101**, 167203 (2008).
 - ³⁴ K. Matan, R. Morinaga, K. Iida and T. J. Sato, *Phys. Rev. B* **79**,

- 054526 (2009).
- ³⁵ Weiqiang Yu, L. Ma, J. Zhang, G. F. Chen, T.-L. Xia, S. Zhang, Y. Hou, arXiv:1004.3581 (unpublished).
- ³⁶ Y. Nakai, K. Ishida, Y. Kmihara, M. Hirano, and H. Hosono, J. Phy. Soc. Jpn. 77, 073701 (2008).